ALLEN INSTITUTE for BRAIN SCIENCE

Allen Mouse Brain Connectivity Atlas

TECHNICAL WHITE PAPER: OVERVIEW

OVERVIEW

The Allen Mouse Brain Connectivity Atlas is a three-dimensional, high-resolution map of neural connections in the mouse brain. Axonal projections from a broad range of brain regions were mapped on a standardized platform to generate a comprehensive database of neural projections. Built upon an array of transgenic mice genetically engineered to target specific cell types, the Allen Mouse Brain Connectivity Atlas (the Atlas) comprises a unique compendium of projections from selected neuronal populations throughout the brain. In addition, the neural connectivity information complements the Allen Institute's gene expression atlases and thus provides opportunities to help understand how genes contribute to connectivity formation and function.

The Atlas is publicly available online via the Allen Brain Atlas data portal (www.brain-map.org) and fully integrated with other Allen Brain Atlas resources. In addition to connectivity data, further characterization of the anatomical expression of transgenes in these mouse lines used to create the Atlas is available, as well as single cell-level data collected from these lines for the Allen Cell Types Database.

The Atlas consists of high resolution 2D image data that can be viewed side-by-side with associated reference datasets, and tools to enable 3D visualization and spatial/ontological search of connectivity models through a combination of manual and informatics analyses. The Atlas includes:

- **Datasets**
  - **Anterograde Projection Mapping:** Axonal projections mapped from ~300 anatomical regions in brain and retina, from diverse neuronal populations defined by ~100 different Cre driver lines or their targets, labeled by viral tracers and visualized using serial two-photon tomography.
  - **Retrograde Input Mapping:** Inputs to visual areas and select associational cortical areas are labeled using a retrograde viral tracer expressing Cre in combination with a Cre-dependent nuclear tdTomato reporter mouse line, and imaged by serial two-photon tomography.
  - **BDA vs. rAAV Comparison:** Axonal projections from 20 brain regions labeled by conventional and viral tracers and imaged with an epifluorescence microscope for direct comparison of the tracing methods.
  - **Transgenic Characterization:** Expression of Cre and other transgenes in ~100 driver and reporter lines revealed in adult and several developmental time points by colorimetric *in situ* hybridization (CISH), fluorescence *in situ* hybridization (FISH) or other histological methods.
  - **Anatomic Reference:** A collection of histology data to better delineate cytoarchitectural details, including fiber tracts.

- **Key features**
  - A 2D and 3D interactive relational database incorporating connectivity information from all brain regions and Cre mice.

- Manual delineation of injection sites for all tracer experiments.
- Development of a Common Coordinate Framework (CCF), an average brain reference space with registration of all projection data and associated 3D reference atlas into this space.
- Signal detection, quantification and other informatics analyses of axonal projections.
- Search and visualization tools for exploring the connectivity data.

STRATEGIES FOR VIRAL- AND CRE-MEDIATED CIRCUIT MAPPING

The use of viral tracers for mapping circuits has distinct advantages over the classic non-viral anterograde tracers such as biotinylated dextran amines (BDA) or phytohemagglutinin (PHA-L).

Anterograde Projection Mapping with Recombinant Adeno-associated Virus (rAAV)

rAAV-mediated expression of fluorescent proteins in infected neurons results in completely labeled cell bodies and axons (Chamberlin *et al.*, 1998). The ability to clearly delineate infected neurons allows one to more precisely quantify infection sites and analyze which neuronal types contribute to axonal projections. rAAV-mediated gene expression is also robust and long lasting; transgene expression can be observed months to years after primary infections in the central nervous system (CNS) (Xiao *et al.*, 1997; Chamberlin *et al.*, 1998; Hadaczek *et al.*, 2010). This feature makes rAAV particularly useful for visualizing very long axonal projections, which is difficult when using other tracers as they begin to degrade after a short period of time. Also, rAAV-mediated cell labeling with bright fluorescent proteins produces robust native fluorescence that can be analyzed with no additional histochemical detection steps which is desirable for dynamic or *in situ* imaging (Bennett *et al.*, 1997; Stettler *et al.*, 2006; Mittmann *et al.*, 2011). Perhaps the greatest advantage of using rAAVs over traditional anterograde tracers is the flexible molecular strategies that can be used to introduce various transgenes into neurons. This enables labeling of selected neuronal populations, such as by combining driver mice that express Cre recombinase under the control of a promoter that displays an interesting expression pattern with a rAAV harboring a Cre-dependent expression cassette. rAAV tract tracing techniques can also be combined with viral-mediated expression of various genetic tool sets, such as channelrhodopsins, to allow functional control of neuronal activity within a network of interest. The recent development and use of intersectional genetic strategies has enabled higher precision for cell-type specific axonal mapping (Gautron *et al.*, 2010; Kravitz *et al.*, 2010). Therefore, rAAV was chosen as the primary anterograde tracer to map anterograde projections from diverse brain regions in various transgenic (Cre driver lines) or non-transgenic mice in this study. The retrogradely transported canine adenovirus 2 expressing Cre recombinase (CAV2-Cre), in combination with local infection of rAAV expressing Cre-dependent EGFP to label axons from specific neuronal populations defined by their targets was also utilized. CAV2 preferentially transduces neurons; it is internalized via its interaction with the coxsackievirus and adenovirus receptor localized within presynaptic terminals (reviewed in Junyent and Kremer, 2015). CAV2 infection produces long-lasting and robust transgene expression in neurons with minimal to no toxicity (Soudais *et al.*, 2001, 2004), and, together with other viral-based tools is useful for analyses of neural circuit architecture (Schwarz *et al*., 2015).

Experimental Considerations

Currently, there are a few important factors that affect the utility of rAAV in tracing experiments. Variability in infection is the most commonly encountered issue when using rAAV as an anterograde tracer. This is due in large part to the underlying mechanisms by which viral particles enter the host cell. Normally, viral entry is mediated by the recognition of cell surface receptors (Wu *et al.*, 2006; Van Vliet *et al.*, 2008). The different affinities of rAAV serotypes for specific cell types are influenced by differences in the capsid proteins that recognize these host cell surface proteins. Each serotype has a unique tropism across different cell types. There are many rAAV serotypes now documented; at least six of which are commonly used to infect different types of neurons in the CNS to varying degrees (Passini *et al.*, 2003; Burger *et al.*, 2004; Cearley and Wolfe, 2007; Taymans *et al.*, 2007; Cearley *et al.*, 2008). Among these, serotype 1 (rAAV2/1; rAAV2 transfer vector is cross packaged with serotype 1 capsid) appears to have the broadest tropism. We also find that serotype 1 indeed infects neurons in the majority of brain regions we have tested (>250). There may still be better serotypes for particular types of neurons that can be determined empirically and will be employed when necessary to supplement the rAAV2/1 vector used in this study. In addition, we have found that iontophoresis of virus greatly

reduces the variability of infection success over multiple experiments, unlike the high amount of variability that can occur with other methods (*e.g.* pressure injection) (Harris *et al.*, 2012). It is unclear at this point if the mechanisms of viral entry into neurons are affected by iontophoresis, which uses a current to drive electrically charged particles out of the pipette.

An additional consideration when using viral vectors is the survival time required to achieve sufficient gene expression. Waiting 2-3 weeks after infection is sufficient for infected neurons to be brightly labeled in both cell bodies and, more importantly for tracing purposes, their axons in bundled tracts and terminal fields. Single fibers can be detected using native fluorescence at this survival time using various imaging methods capable of high resolution.

Many primarily anterograde tracers also result in retrograde transport to some degree. rAAV is no exception, although levels are generally negligible (Chamberlin *et al.*, 1998). Retrograde infection can occur through active transport of the viral genome from synaptic terminals in the area of injection. The amount of retrograde labeling may depend on brain area, cell types, rAAV serotype or viral preparation (Burger *et al.*, 2004; Cearley and Wolfe, 2007; Taymans *et al.*, 2007; Cearley *et al.*, 2008). Using rAAV2/1 and the methods described here, retrograde infection was rarely observed for the majority of brain areas, but notable exceptions include some hippocampal subregions and the globus pallidus.

BDA vs. AAV Comparison

To further address the efficiency and reproducibility of rAAV-mediated tracing methods, a focused set of experiments was designed to compare tracing results from a conventional tracer (BDA) with rAAV. The experimental details are described in the *BDA vs. rAAV* white paper under the Documentation tab, and the data can be found under the BDA/AAV Comparison tab in the Atlas.

BRAIN REGION AND CRE MICE SELECTION

Anterograde Projectome (Brain-wide)

Axonal projections in the adult mouse brain were mapped by two-photon imaging of fluorescently labeled neurons in two distinct phases. In the first phase, Cre-independent viral tracing was performed in C57BL/6J (wild-type) adult mice. Approximately 300 anatomically defined brain regions were chosen from the reference atlas ontology to sample across major structures in the brain. Regions were selected as targets for anterograde tracing based on size (*i.e.*, they were larger than the average viral infection area estimated at 400-700 µm in diameter), surgical accessibility and general scientific interest. Multiple injection sites were allocated for large regions with diverse topography. In the second phase, axonal projections from genetically-defined populations of neurons were studied. Mice engineered to express Cre recombinase under the control of various gene promoters were injected with Cre-dependent rAAV vectors to fluorescently label Cre-expressing neurons and their projections in specific brain regions. The goals were three-fold: (1) map axonal projections from discrete and/or otherwise difficult to access subcortical target areas using anatomically-restricted Cre expression, (2) map projections from specific functional cell types within subcortical brain areas and (3) map axonal projections from neurons in each cortical layer from 40 anatomically-defined cortical areas using mice with laminar-specific Cre expression. Specific Cre lines were identified that were best suited to meet these goals. Information on existing Cre mice was collected and curated from several sources, including GENSAT (http://www.gensat.org/cre.jsp), MGI Cre Portal (http://www.creportal.org/), Cre-X-Mice (http://nagy.mshri.on.ca/cre_new/index.php), MMRRC (http://www.mmrrc.org/catalog/StrainCatalogSearchForm.jsp), NIH Neuroscience Blueprint Cre Driver Network (http://www.credrivermice.org/), the Allen Institute Cre lines (http://connectivity.brain-map.org/transgenic), as well as literature searches for other Cre lines that may not yet be available in the above public repositories. Only Cre mice with transgene expression in the central nervous system, with documented or suspected neuronal expression of Cre, and with biologically interesting or anatomically restricted expression patterns were selected as candidates for further characterization. With these sources and criteria, approximately 340 Cre lines were identified with over 200 unique gene promoters. One hundred of these lines were further characterized in the Transgenic Characterization pipeline, which is an important resource for choosing the most suitable Cre lines and target regions in each line for further study of axonal projections.

Anterograde Projectome (Visual-areas)

To synergize with other Allen Institute projects such as the Allen Cell Types Database, additional data were generated as part of the Allen Mouse Brain Connectivity Atlas to allow more precise mapping of the connectivity between cell types in visual areas of the mouse cortex and thalamus. In the previous Allen Reference Atlas (Dong, 2008), the visual cortex consisted of six areas. In May 2015, a new version of the Allen Mouse Common Coordinate Framework (CCF) was released in which multiple data types were used to improve the delineation of visual cortex, resulting in ten visual areas. Most of these areas can be identified in a living mouse through retinotopic mapping and intrinsic signal optical imaging (ISI). As part of this dataset, ISI was used to guide injections of viral tracers into each desired visual area to provide finer anatomic resolution. Projection data from six locations in primary visual cortex (VISp), spanning visual field space along temporal-nasal and upper-lower axes, and at least five secondary visual areas most robustly identifiable by ISI are planned for inclusion in this Atlas (VISal, VISrl, VISam, VISl, VISpm). Cell type and laminar specificity of projections from each region were mapped using Cre driver mice in combination with Cre-dependent rAAV tracers. In addition to the previously used cytoplasmic EGFP tracer, we have also introduced a new Cre-dependent rAAV for more specific labeling of presynaptic terminals. This virus contains a synaptophysin-EGFP fusion protein.

Target-defined Anterograde Projectome (Visual- and Other Cortical-areas)

To visualize the brain-wide collateralization patterns of output neurons defined by a specific target region (complementing the cell type and laminar specificity achieved through Cre driver lines), we also present projection data from target-defined neuronal populations based on injections of Cre-dependent cytoplasmic EGFP rAAV in visual cortical areas and select other cortical areas in combination with CAV2-Cre injections into a subset of possible target regions (**Figure 1**). Retrograde input maps were obtained as a secondary dataset in these experiments because the dual viral injections were performed in the nuclear tdTomato Cre reporter line, Ai75, which results in all inputs to the target region visualized as tdTomato+ nuclei.

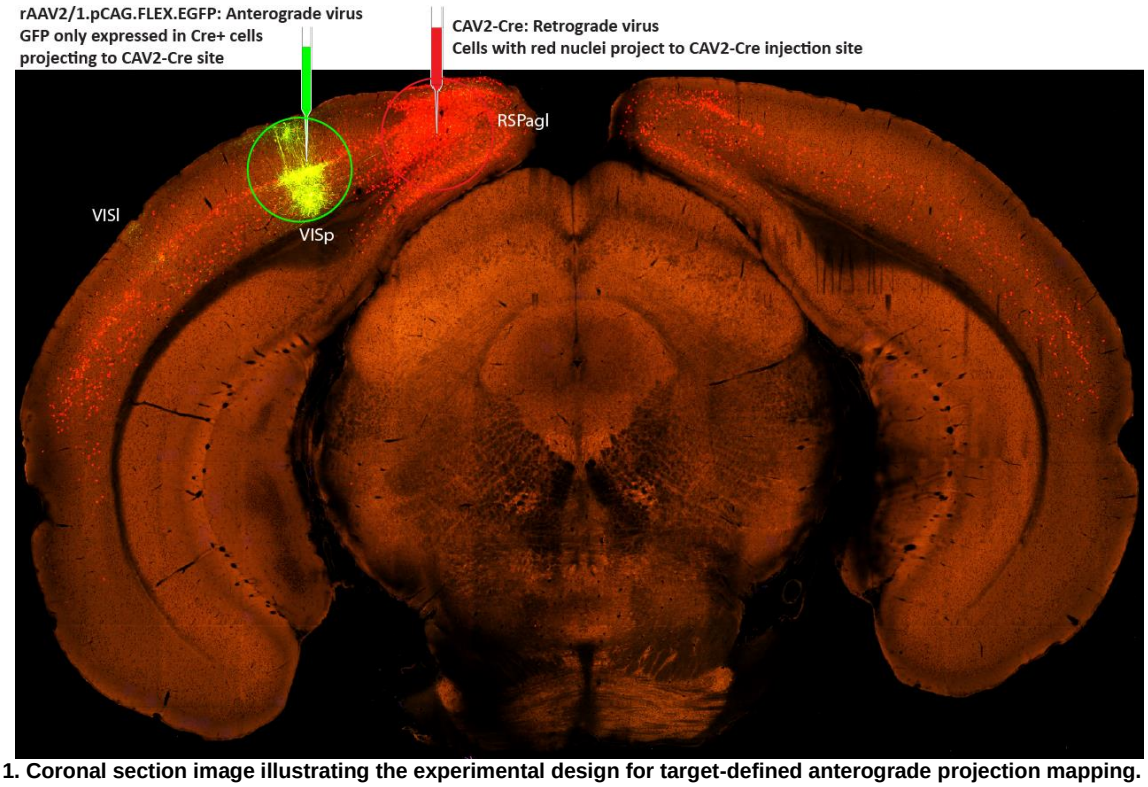

Figure 1. Coronal section image illustrating the experimental design for target-defined anterograde projection mapping.
In this example, CAV2-Cre was injected into the retrosplenial area (RSPagl) and Cre-dependent rAAV was injected into primary visual area (VISp), resulting in GFP expression only in VISp neurons which project to RSPagl. Note collateral projections are visible in the lateral visual area (VISl).

SERIAL TWO-PHOTON TOMOGRAPHY PIPELINE

Axonal projections labeled by viral tracers are systematically visualized through the serial two-photon tomography pipeline (**Figure 2**). By coupling high-speed multi-photon microscopy with automated vibratome sectioning on a dimensionally stable tissue block, this imaging platform greatly reduces deformations commonly occurring with conventional section-based histological methods and provides a series of high-resolution images in pre-aligned 3D space. This approach, offers a strong foundation for the development of 3D tools and connectivity models.

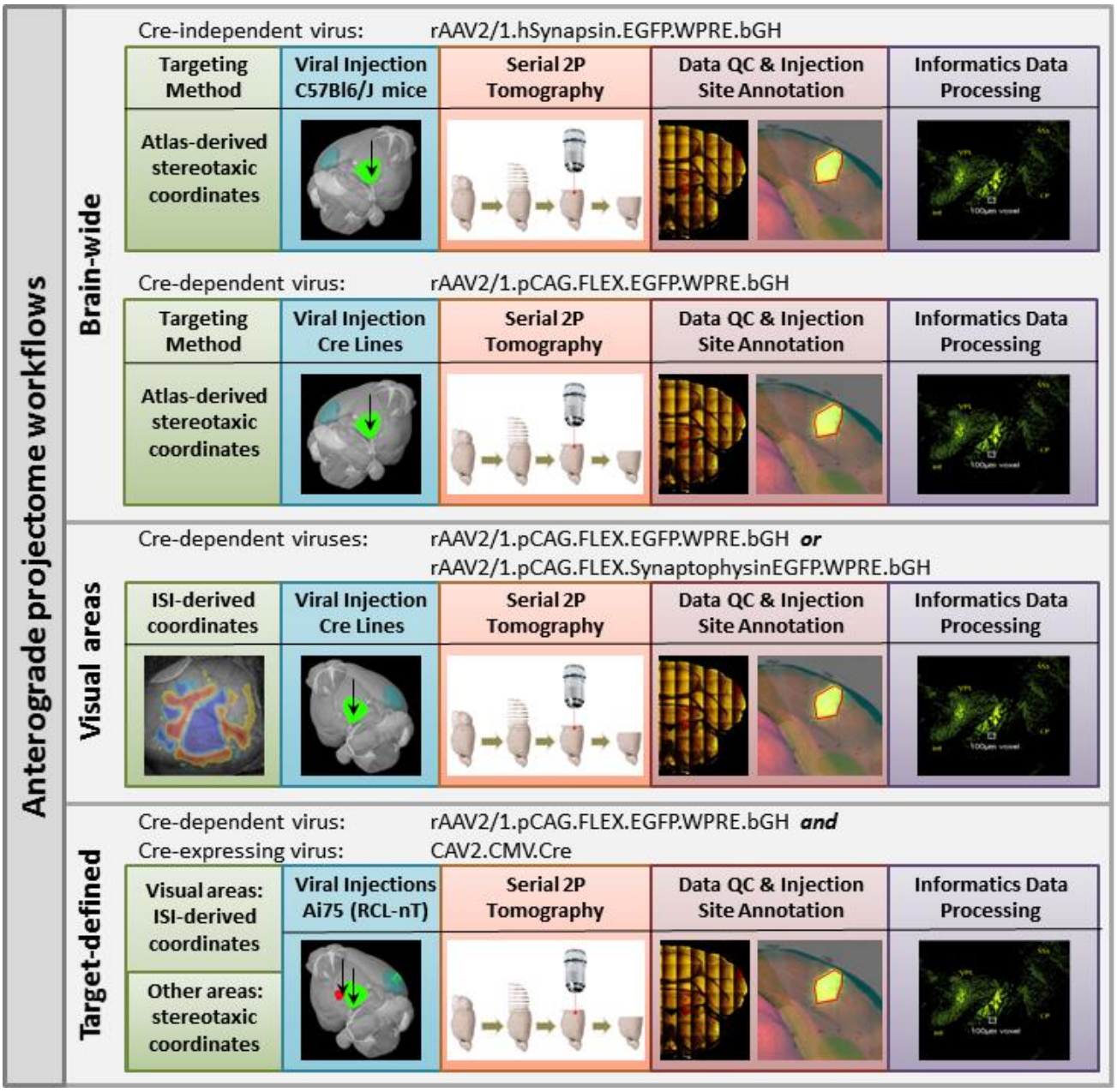

Figure 2. Schematic describing different workflows for brain-wide vs. visual areas anterograde projectome.

Mice

Wild-type adult male C57BL/6J mice (stock 00064) were purchased from The Jackson Laboratory and acclimated to our facility for at least 5 days prior to surgery. Cre driver mice were obtained from various sources as described above, as well as in the *Resources* white paper under the Documentation tab. Cre mice were backcrossed to C57BL/6J mice to minimize genetic variance. For the majority of the study, mice (male and female) backcrossed more than 5 times were used. Ai75 mice were generated at the Allen Institute for Brain Science and are available through The Jackson Laboratory (stock 025106). Mice were group-housed (5 per cage) in micro ventilated cages with a 12 h light/dark cycle. Purina Lab diet 5001 mouse food and water were given *ad libitum*. All surgeries were done in adult mice at postnatal day P56 ± 2. All experimental work described in this white paper was approved by the Allen Institute Institutional Animal Care and Use Committee.

Anterograde Tracers

The rAAV vectors were purchased from the Penn Vector Core (University of Pennsylvania, Philadelphia, PA). Methods used for the packaging, purification and determination of titer of the rAAV vector can be found at http://www.med.upenn.edu/gtp/vectorcore/quality_control.shtml. For brain-wide anterograde projectome mapping, the Cre-independent vector expressed enhanced GFP (EGFP) under control of a human synapsin I promoter with the Woodchuck hepatitis virus post-transcriptional regulatory element (WPRE) and bovine growth hormone polyadenylation sequences (rAAV2/1.hSynapsin.EGFP.WPRE.bGH). The Cre-dependent vector incorporated the flip-excision (FLEX) switch to control expression of EGFP or synaptophysin-EGFP fusion protein from the CAG promoter (rAAV2/1.pCAG.FLEX.EGFP.WPRE.bGH or rAAV2/1.pCAG.FLEX.synaptophysinEGFP.WPRE.bGH). rAAV serotype 1 produced the most widespread tropism throughout diverse brain areas, and was chosen for this study. CAV2-Cre was obtained from the Viral Vector Production Unit at the Universitat Autonoma de Barcelona, and was produced from a vector that enables expression of Cre under control of the CMV promoter.

Targeting and Injections for Brain-Wide Anterograde Projectome

Selection of Stereotaxic Coordinates

Atlas-derived stereotaxic coordinates were chosen for each target area based on *The Mouse Brain in Stereotaxic Coordinates* (Paxinos and Franklin, 2001). For the majority of target sites, the anterior/posterior (AP) coordinates were referenced from Bregma, the medial/lateral (ML) coordinates were distance from midline at Bregma, and dorsal/ventral (DV) coordinates were measured from the pial surface of the brain. For several of the most caudal medullary nuclei (*e.g.*, gracile nucleus and spinal nucleus of the trigeminal, caudal part), the calamus (at the floor of the 4th ventricle) was used as a registration point instead of Bregma. For many cortical areas, injections were made at two depths to label neurons throughout all six cortical layers and/or at an angle to infect neurons along the same cortical column. For laterally located cortical areas (*e.g.* orbital area, medial part; prelimbic area; agranular insular area), the injection was made at two adjacent ML coordinates as the pipette angle required for injection along the cortical column was nearly 90° and technically infeasible.

Stereotaxic Injections of rAAV using Iontophoresis and CAV2-Cre Using Pressure

Mice were anesthetized with 5% isoflurane and placed into a stereotaxic frame (Model# 1900, Kopf, Tujunga, CA). The isoflurane level was maintained at 1-5% throughout the surgery. An incision was made to expose the skull and the skull was leveled with respect to pitch (Lambda and Bregma level), roll, and yaw. A hole was made overlying the stereotaxic coordinates of the targeted area by first thinning the skull using a fine drill burr until only a thin layer of bone remained. A microprobe and fine forceps were used to peel away this final layer of bone to reveal the brain surface. For targeting caudal nuclei in the medulla, ketamine-anesthetized mice were placed in the stereotaxic frame with the nose pointed downward at a 45-60 degree angle. An incision was made in the skin at the base of the skull and muscles were bluntly dissected to reveal the posterior atlanto-occipital membrane overlying the surface of the medulla. A needle was used to puncture the membrane, and the calamus was visualized. All mice received one unilateral injection into a single target region. Glass pipettes (inner tip diameter of 10-20 µm) loaded with virus were lowered to the desired depth from the pial surface of the brain. Currents were applied for iontophoresis of rAAV particles. The majority of injections were done using 3 µA at 7 sec on/7 sec off cycle for 5 min total. A positive current was used with the red (positive) terminal clipped to the

wire in the viral solution and the black (negative) terminal clipped to a clamp on the skin of the mouse. These settings resulted in infection areas of approximately 400 – 1000 µm, depending on target region. Reducing the current strength to 1 µA decreased the area of infected neurons, and was used when 3 µA currents produced infection areas larger than ~700 µm. CAV2-Cre (100-400 nl) was injected via pressure using a Nanoject II system (Drummond Scientific Company). Once the injection was complete, the pipette was withdrawn and, for some mice, the burr hole filled with a small amount of bone wax. For mice that were later to receive ISI-imaging, a headframe and transcranial window surgery was performed immediately following stereotaxic injection (see *Headframe and Transcranial Window Surgery*).

Targeting and Injections for Visual Areas Anterograde Projectome

Cortical visual areas were additionally targeted for tracer injections using functional mapping of visual field space by ISI through the skull, as opposed to stereotaxic coordinates based on skull landmarks.

Headframe and Transcranial Window Surgery

A headframe was attached to the skull to prepare mice for the ISI protocol. Mice were anesthetized with 5% isoflurane and placed into a stereotaxic frame (Model# 1900, Kopf, Tujunga, CA). The isoflurane level was maintained at 1-5% throughout the surgery. An incision was made and skin was removed to expose the skull (including Bregma and Lambda). The skull was then levelled with respect to pitch, roll, and yaw. The stereotax was then zeroed at Lambda using a custom headframe holder equipped with a stylus affixed to a clamp-plate. The stylus was then replaced with the headframe (**Figure 3**) which centers the headframe well at 3.1mm lateral and 1.3mm anterior to Lambda. The headframe was affixed to the exposed skull with white Metabond and once dried, the mouse was removed from the ear bars and placed in a custom clamp to position the skull at a rotated angle of 20 degrees. A 7mm glass coverslip was then placed onto the skull in the center of the headframe well and the glass was levelled and held into place. Clear Metabond was then applied to the underside of the glass coverslip, filling the headframe well and securing the glass to the skull. Black cement was applied to the ridge of the headframe to create a dark, non-reflective surface. As the final step of the headframe surgery, a registered image (photodocumentation) of the transcranial window was collected.

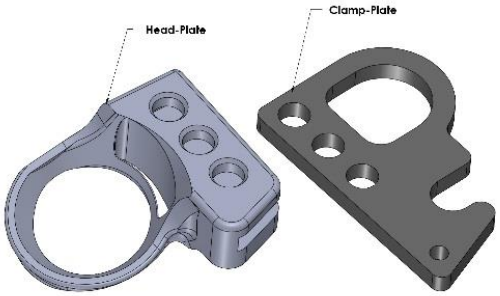

Figure 3. Custom transcranial window headframe.
The headframe consists of a custom-designed 3D-printed head-plate and a stainless steel clamp-plate. Headframes are pre-assembled with Loctite #406 adhesive.

ISI and Sign Map Generation

In a subset of experiments cortical visual areas were targeted for tracer injections using functional mapping of visual field space. ISI was used to measure the hemodynamic response across the cortex to visual stimulation across the entire field of view of an anesthetized mouse. The resulting retinotopic maps were used to delineate visual area boundaries based on visual field sign reversal. Images of the surface vasculature were also used as fiduciary marker to target tracer injection to specific cortical visual area. **Figure 4** shows the workflow of a typical ISI data acquisition session.

Image Acquisition System

To map the functional retinotopic organization of the mouse cortex and standardize data acquisition, an ISI system coupled to visual stimulation was designed and developed. The imaging system illuminated the surface of the mouse cortex with a ring of sequential and independent LED lights, with green (peak wavelength of 527nm and FWHM of 50nm; Cree Inc., C503B-GCN-CY0C0791) and red spectra (peak wavelength of 635nm and FWHM of 20nm; Avago Technologies, HLMP-EG08-Y2000) mounted on the optical lens. The imaging

optics consisted of a pair of Nikon lenses operated front-to-front with a back lens (Nikkor 135mm f/2.8 lens), and a front lens (Nikkor 50mm f/1.8). This set of optics provided a magnification of 2.7X (M = 135/50). The back focal plane of the 50mm lens was adjacent and coplanar to the cranial window providing a working distance of 46.5mm from the flange of the lens. The lens was equipped with a Semrock bandpass filter FF01-630/92nm which limits the reflected light reaching the camera sensor to longer wavelengths. Illumination and image time series acquisition was controlled with an in-house GUI software written in python. Image acquisition was performed with an Andor Zyla 5.5 10tap sCMOS camera. Time series images were captured at a frame rate of 40Hz with frame intervals timed using the camera's hardware clock running at 40MHz. Initiation of simultaneous image acquisition and visual stimulus display was hardware triggered from a National Instruments Digital IO board. Acquired images were 2560X2160 pixel/frame, with 16-bit dynamic range but were saved to disk at a 4X4 spatial binning and 4X temporal binning, 640X640 pixel/frame, 10Hz time series, 32-bit dynamic range and a resulting effective pixel size of 10µm.

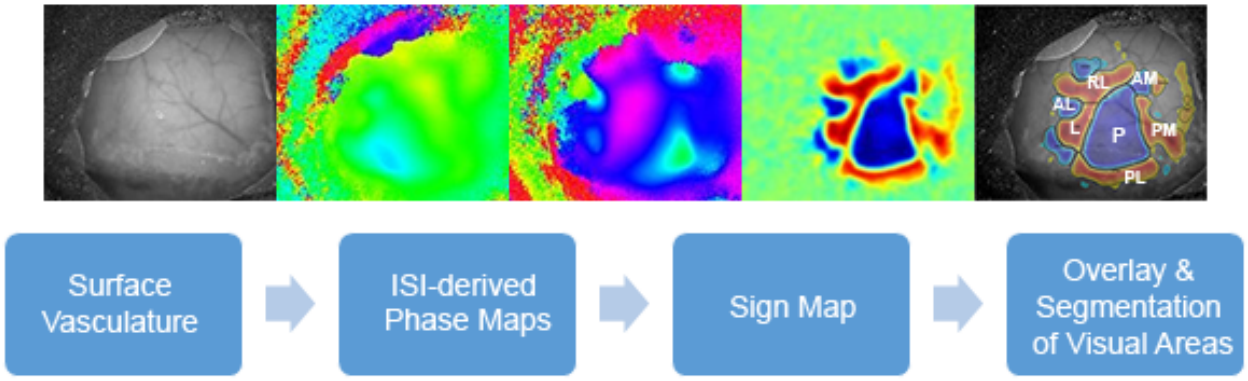

Figure 4. Schematic describing the data acquisition and processing for ISI and sign map generation.
From left to right, a vasculature image was first acquired and vasculature used as fiduciary markers for targeting purpose. Visual stimulus induced ISI was used to generate altitude and azimuth phase maps. Sign maps were obtained from the visual field sign reversal of the phase maps and used to delineate and identified visual areas. Finally, sign maps were auto-segmented and annotated using an algorithm based on previous work by Garrett *et al.* 2014. The resulting segmentation and annotation is shown here overlaid on the vasculature image. Abbreviations: P: primary visual area; L: lateromedial area; AL: anterolateral area; RL: rostrolateral area; AM:anteromedial area; PM: posteromedial area and PL: posterior area.

Animal Preparation

Mice were instrumented with a surgical transcranial window implant (*see Headframe and Transcranial Window Surgery*) exposing the visual area of the cortex on the left hemisphere. Imaging was performed on lightly anesthetized mice with 1-1.4% isoflurane administered with a somnosuite (model #715; Kent Scientific, CON) at a flow rate of 100 ml/min supplemented with ~95% O_2 concentrated air (Pureline OC4000; Scivena Scientific, OR). Vital signs were monitored throughout the experiment with a Physiosuite (model # PS-MSTAT-RT; Kent Scientific). Eye drops (i-drop Vet; Vet Plus Inc.) were applied to keep the eye well hydrated. Mice were placed on a lab jack platform and head frame fixed with the custom transcranial window headframe described above (*see Headframe and Transcranial Window Surgery*) to position the transcranial window at a 23° roll and 6° pitch to normal, allowing the animal to rest in its anatomical position. The head frame and clamping mechanism ensured consistent and accurate positioning of the mouse eye in relation to the stimulus screen from experiment to experiment.

Visual Stimulus

To ensure full coverage of the field of view, a 24" monitor was positioned 10cm away from the right eye and inclined 30° relative to the animal dorsoventral axis. The monitor was also tilted 70° off the horizon to ensure that the stimulus was parallel to the retina of the mice (**Figure 5A**, **5B**). The visual stimulus consisted of a grey background and 20° by 155° bar containing a flickering black and white checker board pattern sweeping 10 times along all four cardinal axis (**Figure 5C**; Kalatsky & Striker, 2003). The visual stimulus was designed so that spherical coordinates could be displayed on a flat monitor (Marshel *et al.*, 2011).

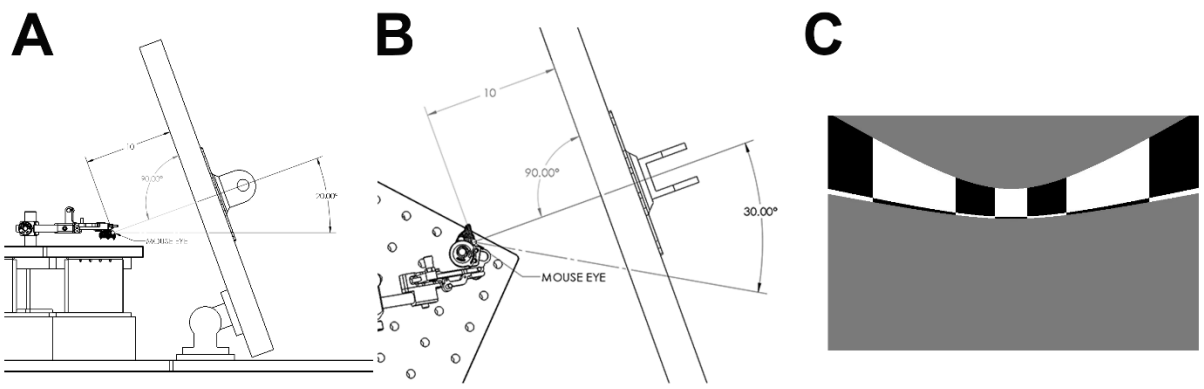

Figure 5. Visual stimulus screen placement and presentation.
(A) Side view of the experimental set up showing the center of the monitor positioned at 10cm away from the eye of the mouse. The monitor was also tilted 70° to the horizontal to present the stimulus parallel to the retina. **(B)** Aerial view of the position of the stimulus monitor showing the screen positioned 30° from the mouse dorsoventral axis also contributing to the parallel relationship between the retina and stimulus display. **(C)** Example snapshot of the stimulus presented, here showing a horizontal sweep moving downwards.

Image Acquisition and Processing

An in focus image of the surface vasculature was first acquired with green LED illumination to provide fiduciary marker reference on the surface of the visual cortex. After defocusing from the surface vasculature, up to 7 independent time series of intrinsic signal images were acquired and used to measure the hemodynamic response to visual stimulus-induced brain activity (see *Image Acquisition System* description above). The resulting images were first processed to maximize the signal-to-noise ratio using time-averaged pixel direct current (DC) signal removal. A Discrete Fourier Transform (DFT) at the stimulus frequency was then performed on the pre-processed images. Phase maps were generated by calculating the phase angle of the pre-processed DFT at the stimulus frequency. The phase maps were used to translate the location of a visual stimulus displayed on the retina to cortical spatial anatomy. A sign map was produced from the phase maps by taking the sign of the angle between the altitude and azimuth map gradients. Averaged sign maps were produced from a minimum of three time series images for a combined minimum average of 30 stimulus sweeps in each direction. Visual area segmentation and identification was obtained by converting the visual field map to a binary image using a manually-defined threshold and further processing the initial visual areas with split/merge routine as previously described in Garrett *et al.* 2014, (see *Automated Sign Map Segmentation and Annotation* below). Sign maps were curated and the experiment repeated if less than 6 visual area including p (Primary Visual Area), L (lateromedial area) and PM (posteromedial area) were positively identified. The sign maps were used to delineate visual areas for targeting injections and annotate projection targets (see *ISI-guided Injection of rAAV Using Iontophoresis*).

Automated Sign Map Segmentation and Annotation

The boundaries and identities of functional visual areas need to be delineated and annotated for targeted viral injection to the center of mass of a visual area or to specific retinotopic coordinates (see *ISI-guided Injection of rAAV Using Iontophoresis*). To determine more objectively the identities of and boundaries between visual areas and to standardize this process for large scale data acquisition, an automated segmentation and annotation module was developed.

A set of 35 ISI experiments was used to train an algorithm developed by earlier work from Garrett *et al*., 2014, to build an initial atlas of 12 major cortical visual areas. For each experiment, the sign map was computed and automatically segmented into distinct visual areas. The identity of each area was then manually annotated. Each sign map was aligned to a canonical space by shifting the center of mass of primary visual area to the

origin, and rotating the image so that the direction of the altitude retinotopy gradient of primary visual area was made horizontal. Using the 35 ISI experiments thus processed, an atlas of the cortical areas was built, and statistics for area sign, location, size and spatial relationships compiled.

Subsequent ISI data were then automatically segmented, and the automated annotation algorithm compared the sign, location, size, and spatial relationships of the segmented areas against those compiled in the atlas. The best match between visual areas in the newly generated sign map and that of the atlas was achieved by minimizing a cost function defined by the discrepancy between the properties of the matched areas, resulting in an auto-segmented and annotated map for each experiment.

The automated ISI segmentation and annotation modules achieved ~97% accuracy on a pilot dataset. To facilitate manual correction and editing of the results, an editing tool was further developed to allow merging and splitting of segmented and annotated areas to correct errors.

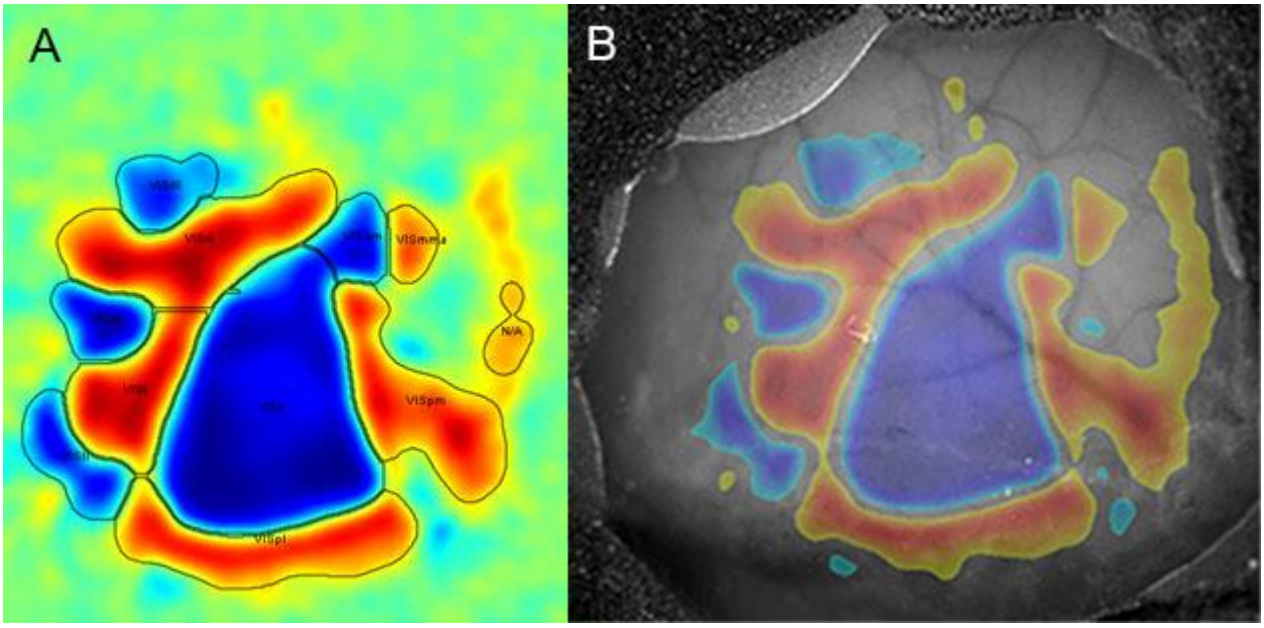

Figure 6. Sign maps used for targeting injections.
(A) Sign map with visual area segmentation and annotation. **(B)** Sign map overlay with surface vasculature image. Targets were selected based on the sign map, and surface vasculature fiducials were used as a guide to target those regions.

ISI-guided Injections of rAAV using Iontophoresis and CAV2-Cre using Pressure

Mice were anesthetized with 5% isoflurane and placed into a stereotaxic frame (Model# 1900, Kopf, Tujunga, CA) equipped with a custom headframe clamp (mounted to the stereotax base) that rotates the headframe by 20 degrees. The isoflurane level was maintained at 1-5% throughout the surgery. The glass coverslip was removed by drilling around the edges to expose the underlying clear Metabond. A small burr hole was drilled first through the Metabond and then through the skull using surface vasculature fiducials obtained from the ISI session as a guide. Drilling around the area of interest was necessary in some cases in order to increase visibility of the reference vasculature through the skull (**Figure 6**). The overlay of sign map on vasculature image was used to identify the target injection site. Once the burr hole over the target location was drilled, a glass pipette (inner tip diameter of 10-20 µm) loaded with virus was lowered to the desired depth from the pial surface of the brain. Currents (3 µA at 7 sec on/7 sec off cycle for 5 min total) were applied for iontophoresis of rAAV particles, or a Nanoject II system was used to deliver 100-400 nl of CAV2-Cre. Once the injection was complete, the pipette was withdrawn and the burr hole was filled with a small amount of bone wax and a glass coverslip was re-affixed to the skull using clear Metabond.

Specimen Preparation

Mice were anesthetized with 5% isoflurane and intracardially perfused with 10 ml of saline (0.9% NaCl) followed by 50 ml of freshly prepared 4% paraformaldehyde (PFA) at a flow rate of 9 ml/min. Brains were rapidly dissected and post-fixed in 4% PFA at room temperature for 3-6 hours and overnight at 4°C. Brains were then rinsed briefly with Phosphate Buffered Saline (PBS) and stored in PBS with 0.02% sodium azide before proceeding to the next step. Agarose was used to embed the brain in a semisolid matrix for serial imaging. After removing residual moisture on the surface with a Kimwipe, the brain was placed in a 4% oxidized agarose solution made by stirring 10 mM $NaIO_4$ in agarose, then transferring through 50 mM phosphate buffer and embedding at 60°C in a grid-lined embedding mold to standardize placement of the brain in an aligned coordinate space (**Figure 7**). The agarose block was then left at room temperature for 20 min to allow agarose to solidify, and then covalent interaction between the brain tissue and the agarose was promoted by placing the block in 0.2% sodium borohydride in 50 mM sodium borate buffer (pH 9.0) for 48 hours at 4°C. The agarose block was then mounted on a 1x3 glass slide using Loctite 404 glue and prepared immediately for serial imaging.

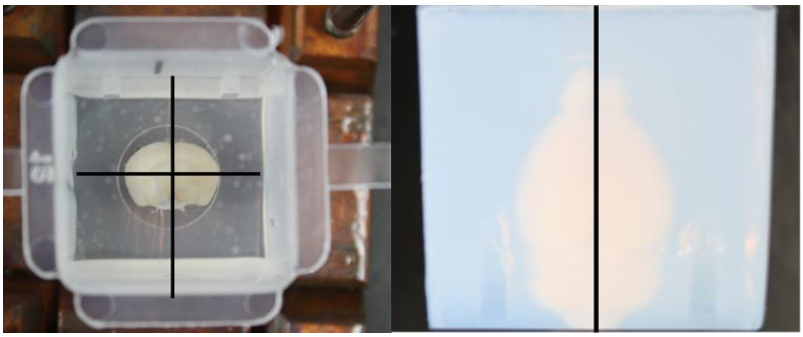

Figure 7. Embedding in agarose.
A brain was aligned in the middle of the agarose block so that the anterior-posterior axis is perpendicular to the bottom and parallel to the vertical axis of the mold. Top (left panel) and side (right panel) views are shown above.

Serial Two-Photon Tomography

Serial two-photon (STP) tomography was developed at the Massachusetts Institute of Technology (Ragan, 2004, 2007) and subsequently commercialized by TissueVision, Inc. (Ragan, 2012). Multi-photon image acquisition for the Atlas was accomplished using the TissueCyte 1000 system (TissueVision, Cambridge, MA) coupled with a Mai Tai HP DeepSee laser (Spectra Physics, Santa Clara, CA).

First, the mounted specimen was placed on the metal plate in the center of the cutting bath as illustrated in **Figure 8**. The cutting bath was filled with PBS with 0.02% sodium azide and placed onto the sample stage. To achieve best results, a new vibratome blade was used for each specimen and aligned to be parallel to the leading edge of the specimen block.

Next, the top surface of the specimen block was brought up to the level of the vibratome blade by adjusting the sample stage height. The z-stage was set to slice at 100 µm intervals. Specimens were oriented for image acquisition to occur from the caudal to the rostral end. Boundaries for each edge of the specimen were defined, such that the XY scan area of the entire brain was estimated. The XY scan area consisted of 204 tiles (17 rows x 12 columns). Each tile was imaged at a resolution of 2080x2080 pixels. The stage moved the tissue block in a serpentine motion to put the next tile under the objective. Imaging of one section can be completed in ~8 min to achieve current resolution of 0.35 µm/pixel. The specimen was illuminated with a 925 nm wavelength laser. The excitation beam was directed to 75 µm below the cutting plane of each specimen by moving the objective using a piezo-controller (Physik Instrumente, Karlsruhe, Germany). This depth was selected as it is deep

enough to minimize deformations at the cutting surface caused by vibratome sectioning but shallow enough to retain sufficient photon penetration for high contrast images. Thus, the optical plane of section is at 75 µm below the slicing surface, with an illumination field area of approximately 3-4 µm ellipsoidal depth.

A Zeiss 20x water immersion objective (NA = 1) was used to focus the light on the sample and to direct fluorescence through the emission path of the system. A 560 nm dichroic (Chroma, Bellows Falls, VT) split the emission light, and a 500 nm dichroic (Chroma) further split the emission for a total of three channels. The 593/40 nm (Chroma), 520/35 nm (Semrock, Rochester, NY) and 447/60 nm emission filter (Chroma) were used for the red, green, and blue channels, respectively. The three photomultiplier tubes (R3896, Hamamatsu, Bridgewater, NJ) were used to detect the emission at each channel. To scan a full tissue section, individual tile images were acquired, and the entire stage (Physik Instrumente) was moved between each tile. After an entire section was imaged, the X and Y stages moved the specimen to the vibratome, which cut a 100 µm section and returned the specimen to the objective for imaging of the next section. The blade vibrated at 60 Hz and the stage moved toward the blade at 0.5 mm/sec during cutting.

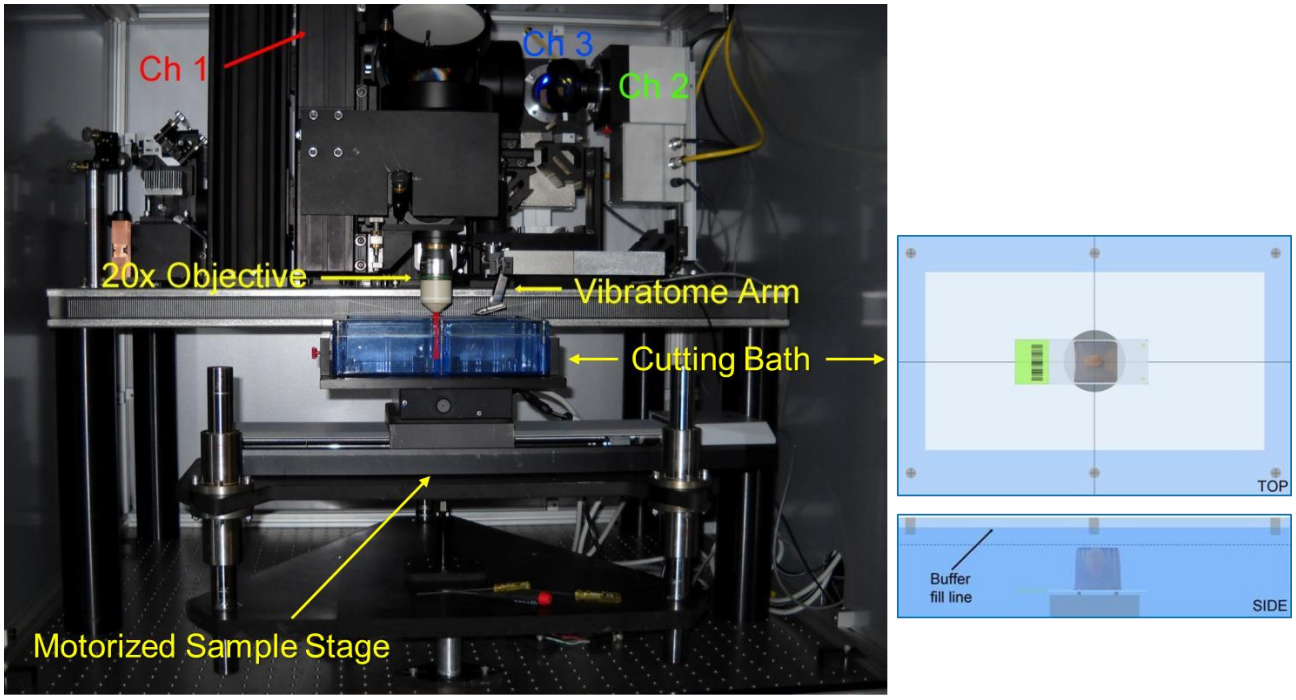

Figure 8. Interior of the TissueCyte 1000 system.
The embedded brain is placed in the middle of the cutting bath so that the leading edge of the agarose block is parallel to the blade (right panel). The cutting bath was filled with PBS-azide buffer and returned to the TissueCyte 1000 system. The motorized sample stage accurately moves the tissue block back and forth between objective lens and vibratome (left panel) to complete imaging of the whole mouse brain.

Images from 140 sections were collected at room temperature to cover the full range of mouse brain. It takes about 18 hours at a resolution of approximately 0.35 µm/pixel. Upon completion of imaging, sections were retrieved from the cutting bath and stored in PBS with 0.02% sodium azide at 4°C.

Data Processing

Once images were acquired, the Informatics Data Pipeline (IDP) managed image stitching, image quality control (QC), annotation QC, and public display of information via the Web application at connectivity.brain-map.org. The IDP has been described in detail previously (Dang *et al.*, 2007), and has been extended to process images

for this project. The Informatics Data Processing whitepaper can be accessed at the Documentation tab on the Website.

Quality Control

Prior to public release of the data, QC was implemented for all serial two-photon tomography data similar to other data modalities. In general, all image series were inspected for artifacts which may reduce consistency, analyzability, or completeness of the data. Severe artifacts such as missing tissue or sections, poor orientation, inadequate injection volume, edge cutoff, tessellation, and low signal strength may cause image series failure.

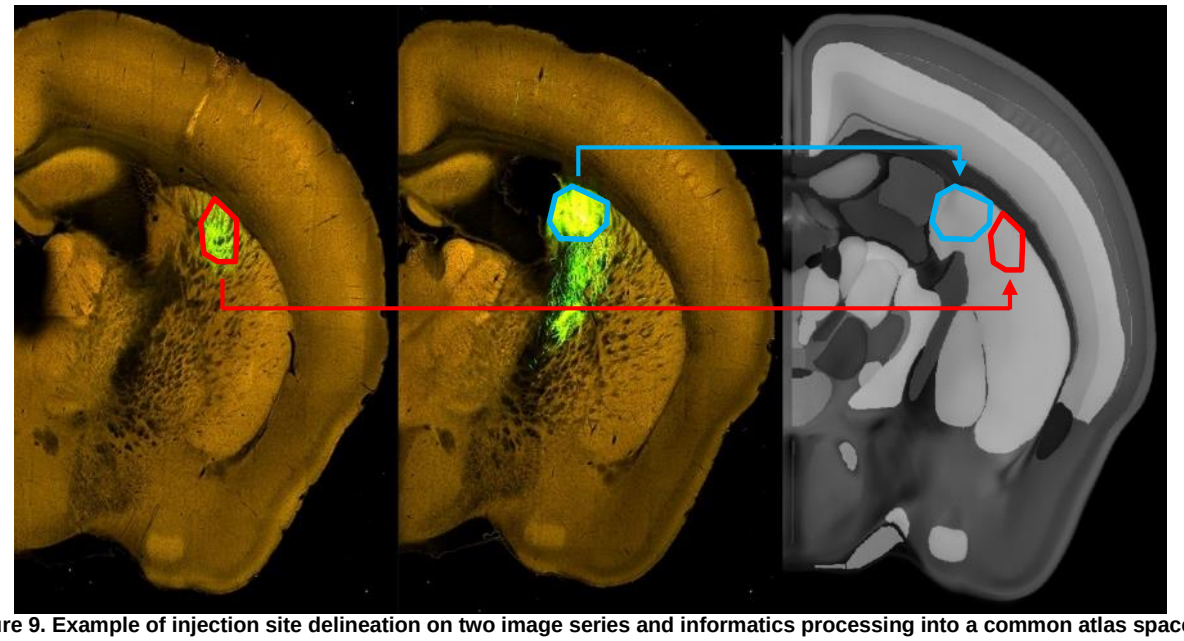

Figure 9. Example of injection site delineation on two image series and informatics processing into a common atlas space. Manually drawn polygons delineate the injection site for two separate image series (left and middle). These polygons are translated into a common atlas space (right) allowing consistent neuroanatomical location of infected structures.

Injection Site Polygon Drawing and Informatics Processing

Once an image series passes the quality control step, injection site polygons are drawn. These polygons are informatically warped into the CCF atlas space as illustrated in **Figure 9**. Green channel signal intensity within the polygons was used to identify which structures have been injected, and to quantify the relative magnitude of their infections. The structure receiving the largest proportion of signal intensity was distinguished as the primary structure, and all other structures were considered secondary structures. A quantified injection summary is provided for each image series that shows the relative amounts of signal detected within each infected structure.

For anterograde projectome data collected from visual areas, an exclusion zone polygon was drawn surrounding the injection site polygon when applicable. The dendrites of infected neurons may create a halo of signal surrounding the injection. The purpose of the exclusion zone was to remove the dendritic contribution to signal intensity for more accurate informatics processing. In the target-defined anterograde projectome datasets, uptake areas for the retrograde CAV2-Cre tracer injections were estimated and delineated using tdTomato nuclear labeling in Ai75 mice. The drawn polygons were registered to the CCF to obtain the relative areal proportion of each infected structure inside the polygon.

REFERENCES

Bennett J, Duan D, Engelhardt JF, Maguire AM (1997) Real-time, noninvasive in vivo assessment of adeno-associated virus-mediated retinal transduction. *Invest Ophthalmol Vis Sci* 38:2857-2863.

Burger C, Gorbatyuk OS, Velardo MJ, Peden CS, Williams P, Zolotukhin S, Reier PJ, Mandel RJ, Muzyczka N (2004) Recombinant AAV viral vectors pseudotyped with viral capsids from serotypes 1, 2, and 5 display differential efficiency and cell tropism after delivery to different regions of the central nervous system. *Mol Ther* 10:302-317.

Cearley CN, Vandenberghe LH, Parente MK, Carnish ER, Wilson JM, Wolfe JH (2008) Expanded repertoire of AAV vector serotypes mediate unique patterns of transduction in mouse brain. *Mol Ther* 16:1710-1718.

Cearley CN, Wolfe JH (2007) A single injection of an adeno-associated virus vector into nuclei with divergent connections results in widespread vector distribution in the brain and global correction of a neurogenetic disease. *J Neurosci* 27:9928-9940.

Chamberlin NL, Du B, de Lacalle S, Saper CB (1998) Recombinant adeno-associated virus vector: use for transgene expression and anterograde tract tracing in the CNS. *Brain Res* 793:169-175.

Dang CN, Sodt A, Lau C, Youngstrom B, Ng LL, Kuan L, Pathak S, Jones AR, Hawrylycz MJ (2007) The Allen Brain Atlas: Delivering neuroscience to the Web on a genome wide scale. *Data Integration in the Life Sciences* in *Lecture Notes in Computer Science* 4544:17-26.

Garrett ME, Nauhaus I, Marshel JH, Callaway EM. (2014) Topography and areal organization of mouse visual cortex. *J Neurosci* 34:12587-12600.

Gautron L, Lazarus M, Scott MM, Saper CB, Elmquist JK (2010) Identifying the efferent projections of leptin-responsive neurons in the dorsomedial hypothalamus using a novel conditional tracing approach. *J Comp Neurol* 518:2090-2108.

Hadaczek P, Eberling JL, Pivirotto P, Bringas J, Forsayeth J, Bankiewicz KS (2010) Eight years of clinical improvement in MPTP-lesioned primates after gene therapy with AAV2-hAADC. *Mol Ther* 18:1458-1461.

Harris JA, Oh SW, Zeng H (2012) Adeno-associated Viral Vectors for Anterograde Axonal Tracing with Fluorescent Proteins in Non-transgenic and Cre Driver Mice. *Curr Protoc Neurosci* 59:1-18.

Junyet F, Kremer EJ (2015) CAV-2--why a canine virus is a neurobiologist's best friend. *Curr Opin Pharmacol* 24:86-93.

Kalatsky VA & Stryker MP (2003) New Paradigm for Optical Imaging: Temporally Encoded Maps of Intrinsic Signal. *Neuron* 38:529–545.

Kravitz AV, Freeze BS, Parker PR, Kay K, Thwin MT, Deisseroth K, Kreitzer AC (2010) Regulation of parkinsonian motor behaviours by optogenetic control of basal ganglia circuitry. *Nature* 466:622-626.

Marshel JH, Garrett ME, Nauhaus I, Callaway EM. (2011) Functional Specialization of Seven Mouse Visual Cortical Areas. *Neuron* 72:1040-1054.

Mittmann W, Wallace DJ, Czubayko U, Herb JT, Schaefer AT, Looger LL, Denk W, Kerr JN (2011) Two-photon calcium imaging of evoked activity from L5 somatosensory neurons in vivo. *Nat Neurosci* 14:1089-1093.

Passini MA, Watson DJ, Vite CH, Landsburg DJ, Feigenbaum AL, Wolfe JH (2003) Intraventricular brain injection of adeno-associated virus type 1 (AAV1) in neonatal mice results in complementary patterns of neuronal transduction to AAV2 and total long-term correction of storage lesions in the brains of beta-glucuronidase-deficient mice. *J Virol* 77:7034-7040.

Paxinos G, Franklin KBJ (2001) *Mouse Brain in Stereotaxic Coordinates*, Second Edition. Elsevier Academic Press, San Diego, CA.

Ragan T, Kim KH, Bahlmann, K, So PT (2004) Two-photon Tissue Cytometry. *Methods in Cell Biology* 75:23-39.

Ragan T, Sylvan JD, Kim KH, Huang H, Bahlmann K, Lee RT, So PT (2007) High-resolution whole organ imaging using two-photon tissue cytometry. *J Biomed Opt* 12:014015.

Ragan T, Kadiri LR, Venkataraju KU, Bahlmann K, Sutin J, Taranda J, Arganda-Carreras I, Kim Y, Seung HS, Osten P (2012) Serial two-photon tomography for automated *ex vivo* mouse brain imaging. *Nat Methods* 9:255-258.

Schwarz LA, Miyamichi K, Gao XJ, Beier KT, Weissbourd B, DeLoach KE, Ren J, Ibanes S, Malenka RC, Kremer EJ, Luo L (2015) Viral-genetic tracing of the input-output organization of a central noradrenaline circuit. *Nature* 524:88-92.

Soudais C, Laplace-Builhe C, Kissa K, Kremer EJ (2001) Preferential transduction of neurons by canine adenovirus vectors and their efficient retrograde transport in vivo. *FASEB J.* 15:2283-2285.

Soudais C, Skander N, and Kremer EJ (2004) Long-term in vivo transduction of neurons throughout the rat CNS using novel helper-dependent CAV-2 vectors. *FASEB J.* 18:391-393.

Stettler DD, Yamahachi H, Li W, Denk W, Gilbert CD (2006) Axons and synaptic boutons are highly dynamic in adult visual cortex. *Neuron* 49:877-887.

Taymans JM, Vandenberghe LH, Haute CV, Thiry I, Deroose CM, Mortelmans L, Wilson JM, Debyser Z, Baekelandt V (2007) Comparative analysis of adeno-associated viral vector serotypes 1, 2, 5, 7, and 8 in mouse brain. *Hum Gene Ther* 18:195-206.

Van Vliet KM, Blouin V, Brument N, Agbandje-McKenna M, Snyder RO (2008) The role of the adeno-associated virus capsid in gene transfer. *Methods Mol Biol* 437:51-91.

Wu Z, Asokan A, Samulski RJ (2006) Adeno-associated virus serotypes: vector toolkit for human gene therapy. *Mol Ther* 14:316-327.

Xiao X, Li J, McCown TJ, Samulski RJ (1997) Gene transfer by adeno-associated virus vectors into the central nervous system. *Exp Neurol* 144:113-124.